

Characterization of Electron Beam Physical Vapor-Deposited Thermal Barrier Coatings Using Diffuse Optical Reflectance

Andi M. Limarga* and David R. Clarke

Materials Department, College of Engineering, University of California, Santa Barbara, California 93106-5050

The use of diffuse optical spectral reflectance as a nondestructive tool to characterize the microstructure of electron beam physical vapor deposition (EB-PVD) thermal barrier coatings (TBCs) has been investigated and the contributions of inter-columnar gaps and intracolumnar pores distinguished. It is shown that the reflectance is controlled by the refractive index mismatch and that the optical scattering coefficient depends on the thickness of the TBC due to the porosity distribution through the thickness of the coating. The sensitivity of the reflectance to the porosity suggests that optical reflectance can be used to characterize the microstructure of EB-PVD TBC for both quality control and nondestructive evaluation purposes.

Introduction

Thermal barrier coatings (TBCs) are used to provide thermal protection to metallic components in a turbine engine from the harsh high-temperature environment. Typically, a TBC consists of a 7 wt% yttria-stabilized zirconia (7YSZ) layer deposited by either air plasma spray (APS) or electron beam physical vapor deposition (EB-PVD) on bond-coated superalloys. During deposition process, a thin layer of thermally grown oxide (TGO) consisting of alumina scale develops at the interface between the TBC and the bond coat and it thickens during high-temperature service. Different microstructures are produced by the two processes: APS has a splat-like structure with interfaces parallel to the

metal/coating interface while an EB-PVD TBC has a columnar structure growing perpendicular to the interface. Primarily for this reason, APS TBCs have lower thermal conductivity than EB-PVD TBCs. However, the columnar structure, with distinct intercolumnar gaps, enhances the mechanical compatibility of the coating with the underlying metallic substrate upon cycling to high temperature.¹

In addition to the low intrinsic thermal conductivity of YSZ, the thermal protection efficiency of TBC relies on the volume fraction and shape of the porosity in the coating.^{2–4} The importance of the porosity can be appreciated when the thermal conductivities of APS and EB-PVD coatings of 7YSZ, which are typically reported to be 0.8–1.1 and 1.5–1.9 W/(m K),⁵ respectively, are compared with the thermal conductivity of a dense 7YSZ, which is 2.5–3.0 W/(m K) at room temperature.^{6,7} Typically, the reduction of thermal conductivity

*limarga@engineering.ucsb.edu

afforded by the presence of porosity is attributed to the decrease of net-section area through which heat can be transported by phonons.⁸

During service at high temperatures, the microstructure of the coatings can change as a result of coarsening and sintering, and possibly densification (Fig. 1). These processes can also lead to an increase in the thermal conductivity of the coatings and consequently an increase in the temperature of the coated metal component that the coating is designed to insulate. In addition, staining and coloring of the coating can occur as a result of contamination from the combustion gases, which can also affect the temperature distribution within the coating. For these reasons, it would be desirable to have a nondestructive method of monitoring microstructural changes in the coating as well as any changes in the optical absorption at wavelengths associated with contamination. Diffuse optical reflectance as a function of wavelength has the potential of being able to quantify these changes and to serve as a noncontact, nondestructive evaluation tool. Optical reflectance measurements are promising because they can be applied to real components as well as flat test coatings. While studies on optical properties of materials typically involve both reflectance and transmittance, the latter was ruled out because the TBCs are applied on metallic components, which block optical transmission. The objective of this exploratory study was to evaluate the feasibility of using diffuse optical reflectance as a nondestructive tool for characterizing EB-PVD TBCs. This has involved an evaluation of dominant microstructural features that

influence optical reflectance and the application of the optical reflectance technique to follow microstructural evolution during thermal cycling.

Optical Scattering in EB-PVD TBCs

The extensive light scattering by an EB-PVD TBC in visible spectral region results in the white appearance of the coating in ambient lighting, compared with the transparency of a zirconia single crystal. Essentially, pure stabilized zirconia crystals are transparent in the wavelength range of about 0.35–5 μm and polycrystals are translucent over the same range.^{9,10} The optical scattering in an EB-PVD TBC has been discussed previously¹¹ but the basic mechanisms are outlined here for illustrative purposes. When light is incident on the columnar structure of EB-PVD TBC, scattering results from: (i) reflection from the surface; (ii) reflection from the interface between the pores and the medium; (iii) refraction in the pores; and (iv) diffraction (Fig. 2). The refracted light may be partially absorbed and refracted out of the pore. These processes are repeated as the light intercepts another pore/interface. Essentially, optical scattering within the coating consists of multiple reflections and refractions as light propagates in the coating. In the limit of multiple scattering events, the light essentially diffuses through the coating until reflected back out of the coating. Light scattering in a medium is typically characterized by the scattering coefficient. This parameter is inversely related to an effective scattering

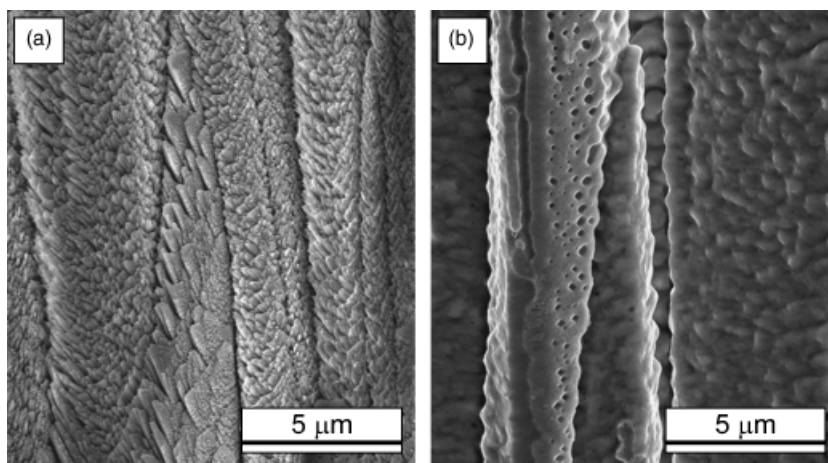


Fig. 1. Surface morphology of thermal barrier coating (TBC) columns in (a) their as-deposited condition and (b) after 200 h at 1150°C. The initial feathery structure evolves to a smoother surface and some large pores were observed inside the column.

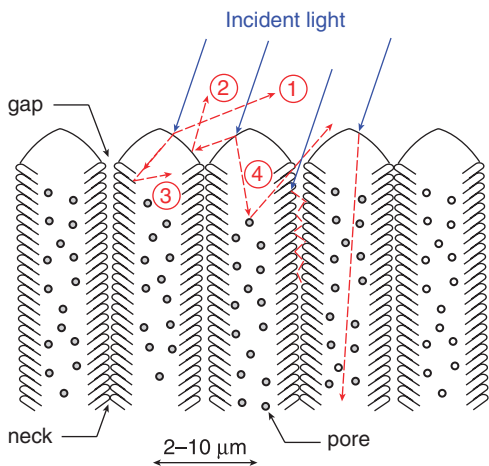


Fig. 2. Schematic illustration of the multiple paths that incident light experiences in propagating through a porous electron beam physical vapor deposition (EB-PVD) thermal barrier coating (TBC). Light can be reflected from the surface of the TBC (path 1), multiply reflected from the TBC/air interface (path 2), refracted into the TBC column, and then scattered by the interface in the gaps (path 3) or by internal pores (path 4). Adapted from Li and Clarke.¹¹

length: the mean distance traveled by a photon between scattering collisions.¹² It is akin to the mean free path for other diffusive processes, such as thermal conductivity and electrical conductivity.

Experimental Details

Specimen

Standard furnace cycle test coupons were provided by Howmet Corporation (Whitehall, MI) in the form of 140- μm -thick EB-PVD 7YSZ coatings deposited on platinum-modified nickel-aluminide-coated single crystal superalloys (25.4 mm diameter, 3 mm thick). Several companion coupons but without a TBC were used to determine the optical properties of the bond coat after oxidation for different times to produce TGO of different thickness.

The effect of TBC thickness on optical scattering was evaluated by performing successive reflectance measurements upon removal of a certain thickness of TBC by polishing with 800-grit SiC paper. Cross-sectional cuts were made near the edges on the opposite sides of the specimen to allow TBC thickness measurement using an optical microscope. The thickness variation from one to the opposite edge of the specimen was $< 10 \mu\text{m}$.

In order to evaluate the effect of refractive index mismatch at the intercolumnar gaps, the reflectance of a TBC coupon after infiltration under vacuum with epoxy was measured and then the reflectance was recorded as the infiltrated coating was successively polished away.

Thermal Cycling Experiment

To evaluate the evolution of optical reflectance with thermal cycling, coupons were cycled (up to 200 cycles) from room temperature to 1150°C in ambient atmosphere. Each cycle consisted of 1-h exposure at 1150°C and 10-min cooling to room temperature. The heating and cooling rates were approximately 200°C/min. The specimen was periodically removed from the thermal cycle rig for optical reflectance measurement. The microstructures of the coating in its as-deposited condition and after 200 cycles were evaluated using scanning electron microscopy.

Diffuse Reflectance Measurement

Diffuse reflectance measurements were performed at room temperature using a UV-VIS-NIR spectrophotometer (UV3600, Shimadzu, Tokyo, Japan) equipped with an integrating sphere (60 mm internal diameter, coated with BaSO_4). Halogen and deuterium lamps were used as the light source to provide directional radiation to the specimen (normal to the surface) and the hemispherical reflected light from 250 nm up to 2500 nm was collected by two types of detectors: a photomultiplier tube for the UV/VIS and a PbS detector for the NIR range. As the measured reflectance was relative to the reflectance of BaSO_4 , the magnitude of spectral reflectance was also calibrated using NIST-calibrated diffuse reflectance standards (Spectralon, LabSphere, North Sutton, NH).

Results

Synopsis of Spectral Diffuse Optical Reflectance of EB-PVD TBC

Figure 3 shows the spectral reflectance from a variety of 7YSZ samples, each having their own characteristic microstructures. The reflectance of an APS TBC was similar to that of a dense polycrystalline 7YSZ, namely a high reflectance over almost the entire wavelength range from 400 to 2500 nm and decreasing

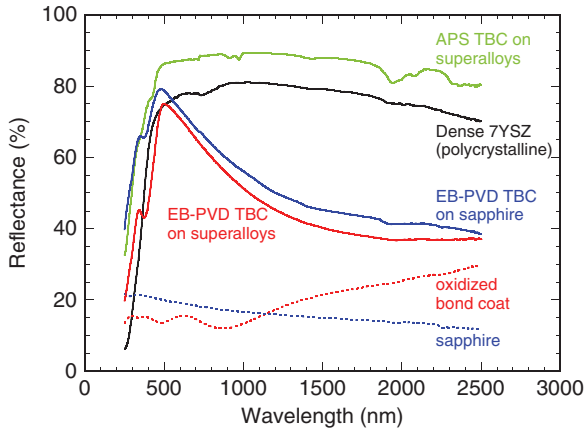


Fig. 3. Spectral diffuse reflectance of 7YSZ with various microstructures. The discontinuity at $\lambda = 720$ nm is an experimental artifact due to the switching of the monochromator grating.

rapidly due to the absorption edge of 7YSZ at about 400 nm. While the EB-PVD TBC had a similar high reflectance in the visible (around 500 nm) to those of APS and dense polycrystalline zirconia, the shape of its spectral reflectance was noticeably different. In particular, the reflectance of the EB-PVD coating at high wavelength ($\lambda > 1500$ nm) was very low compared with those of APS and dense YSZ. These observations indicated that the optical scattering and its wavelength dependence are strongly influenced by the microstructure of the coating.

Determination of Scattering Coefficient in EB-PVD TBCs

An accurate determination of scattering and absorption coefficients of a material or coating normally requires both reflectance and transmittance measurement of specimens with different thicknesses.^{10,13,14} This is feasible for an APS coating because a coating can be sprayed onto a sacrificial substrate but proves to be difficult to implement in an EB-PVD coating for two reasons. First, a thin freestanding EB-PVD coating is extremely fragile making it difficult to handle. Second, the microstructure of an EB-PVD coating depends on the position within the coating and the size of the TBC columns grows during deposition.¹⁵ This is thought to be responsible for the thickness dependence of thermal conductivity in an EB-PVD TBC coatings reported by several groups.¹⁶

In order to estimate the scattering coefficient of the coatings, we adopted a procedure originally proposed by Scallan to analyze the spectral reflectance of paper.¹³ In this approach, the coating is considered as a stack of thin layers placed upon a background and the reflectance calculated as the number of layers in the stack is increased. Scallan's method is, in effect, a discrete description that reduces to the better-known Kubelka–Munk continuum equations. The reflectance R of a coating of thickness h can be calculated from the integral of the scattering of the individual layers as follows¹³:

$$\int_{R_{bg}}^R \frac{dR}{1 - 2(1 + k/s)R + R^2} = \int_0^h s \cdot dh \quad (1)$$

where R_{bg} is the reflectance of the back ground, k is the absorption coefficient, and s is the scattering coefficient. In this equation, as well as in the Kubelka–Munk equation, the refractive indices of the coating materials and the pores do not enter in a simple manner because the coating is, in essence, considered a composite medium. It is worth noting that the reflectance also depends on the shape, size, and distribution of the pores. The reflectance at different wavelengths can then be used to determine the wavelength dependence of the scattering and absorption coefficients. For zirconia, over the wavelength range of 400–2500 nm, the absorption coefficient is several orders magnitude lower than the scattering coefficient and so can be neglected.^{10,14} In order to proceed with the analysis without having to introduce unnecessary assumption and adding unwarranted complexity, it was further assumed that the value of the scattering coefficient is not dependent on the coating thickness but only on the wavelength. Thus the scattering coefficient of the coating can be written as

$$s = \frac{1}{h} \frac{R - R_{bg}}{(1 - R)(1 - R_{bg})} \quad (2)$$

where R is the measured reflectance of the thermal barrier-coated specimen. R_{bg} was independently measured on a grit-blasted bond coat on a superalloy coupon without TBC that was also oxidized at 1150°C to form a thin thermally grown alumina scale (the spectral reflectance of bond-coated coupon without TBC after oxidation at 1150°C was also shown in Fig. 3). It is emphasized that it is assumed that the scattering coefficient is uniform through the thickness of the TBC. Thus, this value refers to the average scattering coefficient of the coating.

Effect of TBC Thickness on Optical Scattering

The reflectance of EB-PVD TBC with progressive reduction in the coating thickness by fine polishing is shown in Fig. 4. Over almost the entire wavelength range (500–2500 nm) the reflectance decreased with decreasing thickness. However, the analysis using Eq. (2) indicated that the scattering coefficient increases with decreasing thickness, particularly in the ultraviolet and visible regions (Fig. 5). The scattering coefficient at higher wavelength was essentially unchanged. It was observed that the area around the reflectance peak (at about 500 nm) became sharper with polishing.

Effect of Intercolumnar Gaps on Optical Scattering

Figure 6 shows the reflectance of an EB-PVD TBC that had been infiltrated by epoxy, followed by polishing away portions of the coating thickness. After removing the excess of epoxy from the top surface, it was observed that the reflectance of the specimen was reduced by approximately 10–15%. Further polishing of the infiltrated sample showed the same trend with the uninfiltrated TBC, namely a decrease in reflectance with decreasing TBC thickness. Similarly, the scattering coefficient of the TBC upon epoxy infiltration was reduced while the polishing step increased the scattering coefficient (Fig. 7).

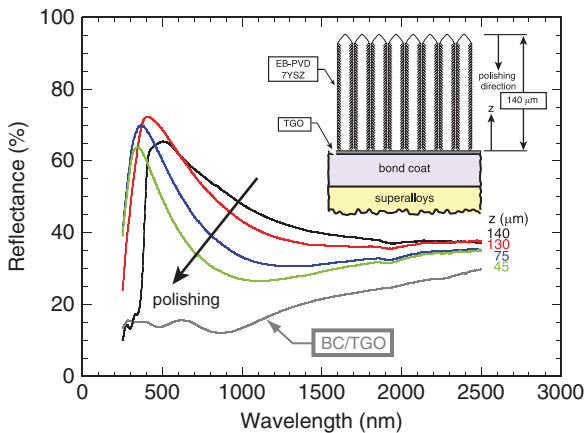


Fig. 4. Effect of thermal barrier coating (TBC) thickness on spectral diffuse reflectance. The reflectance of oxidized bond-coated superalloys without any TBC that was used as the reflectance of the background in determining the scattering coefficient was also shown. *z* indicates the remaining TBC thickness after polishing away the top of the coating.

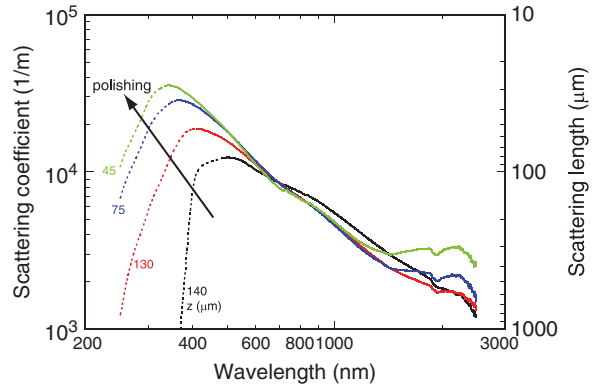


Fig. 5. Scattering coefficient of electron beam physical vapor deposition (EB-PVD) thermal barrier coating (TBC) as a function of the coating thickness calculated from reflectance measurement (shown in Fig. 4). The scattering length was defined as (1/scattering coefficient).

Effect of Thermal Cycling on Optical Scattering

The evolution of the spectral reflectance with thermal cycling is shown in Fig. 8. The as-received TBC coupon showed a relatively lower reflectance than those after thermal cycling. One-hour heat treatment at 1150°C immediately increased the reflectance and altered the shape of the spectral reflectance, which then continued to evolve with thermal cycling. A maximum

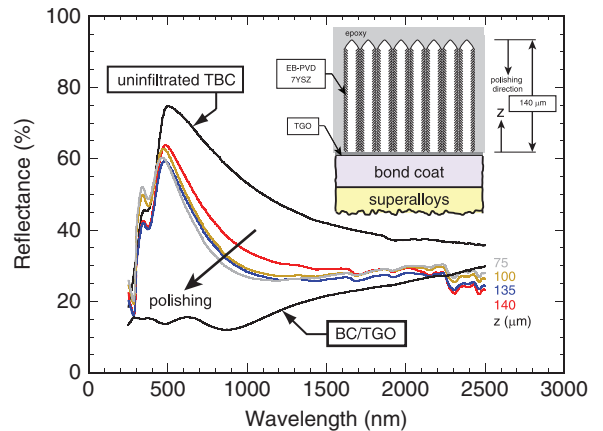


Fig. 6. Spectral reflectance of a 140-μm-thick electron beam physical vapor deposition (EB-PVD) thermal barrier coating (TBC) infiltrated with epoxy followed by polishing off the top of the coating. *z* indicates the remaining TBC thickness after polishing away the top of the coating.

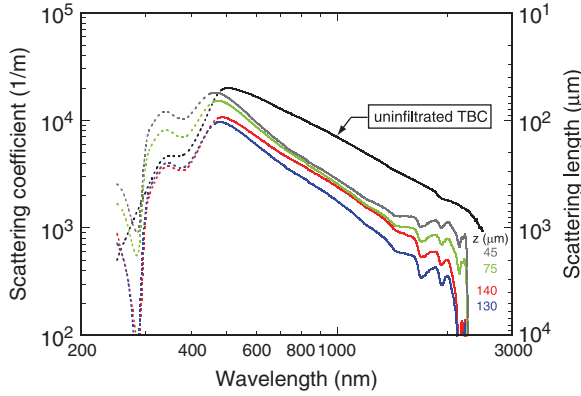


Fig. 7. Scattering coefficient of epoxy-infiltrated electron beam physical vapor deposition (EB-PVD) thermal barrier coating (TBC) calculated from reflectance measurement (Fig. 6).

reflectance was observed at around 500 nm. Below this wavelength, the reflectance did not change significantly with thermal cycling. By contrast, the reflectance above 500 nm increased monotonically with thermal cycling (Fig. 9a). The peak position shifted to a longer wavelength but its magnitude also decreased with thermal cycling (Fig. 9b). Similar trends were also observed in the value of the scattering coefficient calculated from the reflectance measurement (Fig. 10).

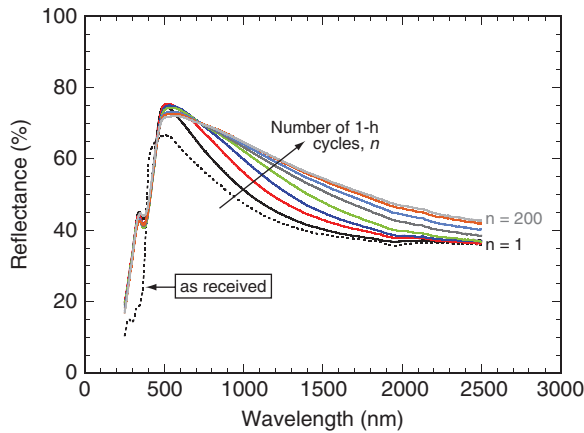


Fig. 8. Effect of thermal cycling on spectral diffuse reflectance of electron beam physical vapor deposition (EB-PVD) thermal barrier coating (TBC). The number of 1-h cycles, n is successively 1, 5, 10, 20, 50, 100, 150, and 200.

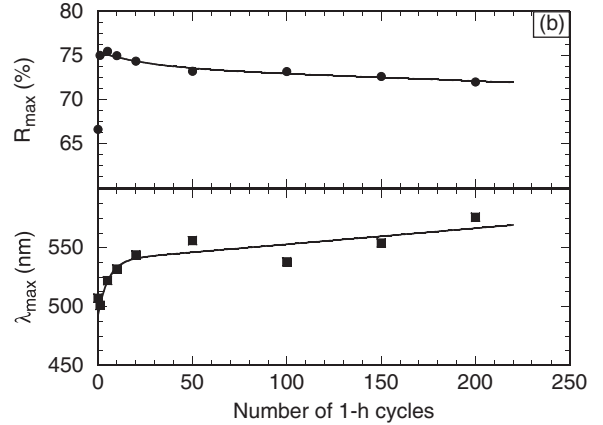
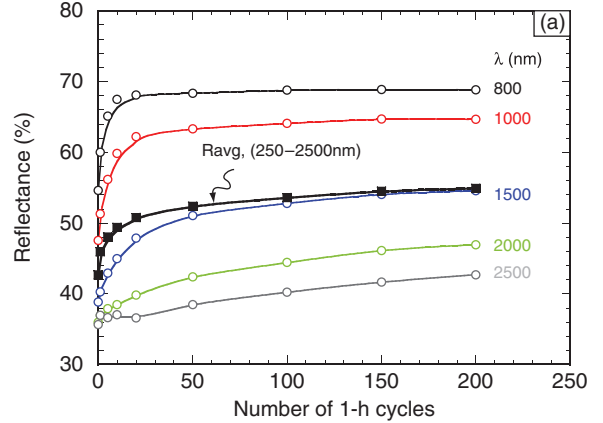


Fig. 9. Distinct features in the evolution of spectral reflectance with thermal cycling: (a) increase of reflectance at various wavelengths and (b) shift of the peak in spectral reflectance with thermal cycling.

Discussion

The objective of this work was to explore the feasibility of using diffuse optical reflectance for the characterization of TBCs deposited by electron beam evaporation. As mentioned earlier, the diffuse reflectance is dominated by multiple reflections as light propagates in the coating. Light is scattered by a number of distinct microstructural features, for example surface roughness, porosity inside the TBC column, feathery structure on the wall of the column, and intercolumnar gaps. In addition to the geometrical effects, the optical scattering is controlled by the refractive index mismatch between zirconia and the medium inside the porosity, for instance air.

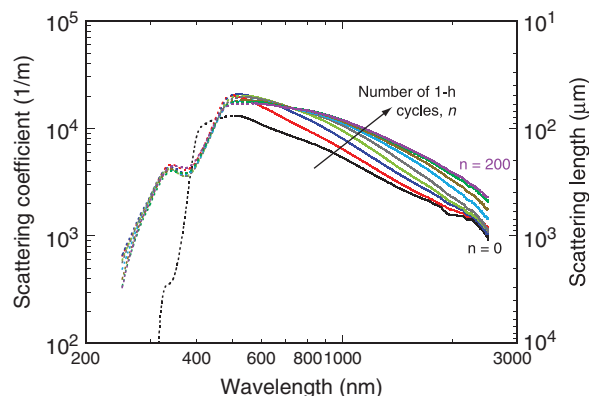


Fig. 10. Evolution of scattering coefficient of electron beam physical vapor deposition (EB-PVD) thermal barrier coating (TBC) with thermal cycling. The number of 1-h cycles, n is successively 1, 5, 10, 20, 50, 100, 150, and 200.

Figure 3 suggested that despite the translucency of polycrystalline YSZ in the visible–near-infrared regions of the spectrum, the reflectance of an EB-PVD TBC is dominated by the TBC itself and not by the underlying substrate. This can be seen by the similar spectral reflectance, both in terms of shape and magnitude, of EB-PVD TBC deposited on sapphire and bond-coated superalloys. To verify this observation, the reflectance of a freestanding EB-PVD TBC (obtained from a TBC coupon that had spalled after being thermally cycled to failure) was investigated. To further investigate the effect of the underlying substrate, the freestanding TBC was placed on a black background having reflectance $<4\%$ over the entire range of measured wavelength. Despite the slight difference in magnitude, it was clear from Fig. 11 that all EB-PVD TBCs have similar shape of the spectral reflectance irrespective of the substrates on which they are covering. The small difference in reflectance magnitude of the freestanding coating was attributed to the illuminated area being smaller than the beam size ($5 \times 6 \text{ mm}^2$), hence, resulting in a lower reflectance.

Having established that the reflectance of a TBC coupon is dominated by the reflectance of the coating rather than by that of the underlying substrate or by interfacial gap between the coating and the substrate, contributions from the pores in the TBC columns and intercolumnar gaps to optical scattering were examined. Both these microstructural features are responsible for the multiple reflections due to refractive index mismatch between zirconia and air.

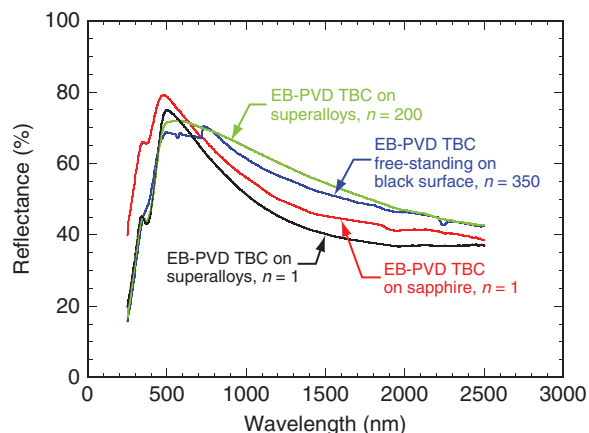


Fig. 11. Spectral reflectance of electron beam physical vapor deposition (EB-PVD) 7YSZ deposited on superalloys and sapphire. The freestanding EB-PVD thermal barrier coating (TBC) was in the form of fragmented segments of EB-PVD TBC on superalloys that has undergone major spallation after 350 cycles (n in the legend refers to the number of cycles at 1150°C). The discontinuity at $\lambda = 720 \text{ nm}$ is an experimental artifact due to switching of monochromator grating.

Effect of Porosity Distribution in EB-PVD TBCs on Optical Scattering

Analysis of the reflectance and scattering coefficients indicates that the wavelength-dependent scattering coefficient of TBC depends on TBC thickness (Fig. 5). Specifically, the scattering coefficient increased with decreasing thickness at $\lambda < 600 \text{ nm}$. Furthermore, it was also observed that the peak of the scattering coefficient shifted to a shorter wavelength with a higher magnitude. This observation is consistent with the column size distribution through the thickness of the coating. Near the bond coat/TBC interface, the TBC columns are much smaller than those near the TBC top surface.^{6,15,17} As depicted in Fig. 2, random spherical pores (approximately 20 nm in diameter) have also been observed inside individual TBC columns.^{4,15} Furthermore, the feathery structure of the TBC columns, associated with successive depositions as the coupons rotate in front of the EB source, is also dependent on the position within the coating. This feathery structure extends to about 1/3–1/2 the column radius, followed by oblate and prolate spheroidal pores parallel to the feathery structure.⁴ Observation using small-angle X-ray scattering revealed that the density of this type of porosity is larger at the TBC/TGO interface.¹⁸ As the number of

light scattering centers, intracolumnar pores and gaps alike, increases closer to the interface with the alloy, the scattering coefficient can also be expected to increase.

The calculated scattering coefficient in an EB-PVD TBC was found to be significantly smaller than that in an APS TBC. As an example, the scattering coefficient at $\lambda = 1 \mu\text{m}$ found in this study was $6.4 \times 10^3 \text{ m}^{-1}$ while the reported scattering coefficient in an APS TBC is about 10^5 m^{-1} .¹⁵ Based on Siegel's analysis,¹⁹ this comparison suggests that radiative heat transfer through an EB-PVD TBC is much greater than through APS TBCs.

Effect of Refractive Index Mismatch at the Inter-columnar Gaps on Optical Scattering

The second major contributor to the optical scattering in an EB-PVD TBC is the refractive index mismatch between air and zirconia at the intercolumnar gaps. For the sake of illustration, we have referred to the angle-integrated average of the Fresnel equation to calculate the hemispherical reflectance of a two-phase material (ρ_d^{ext}), each with different optical properties^{14,20}:

$$\rho_d^{\text{ext}} = \frac{1}{2} + \frac{(3n+1)(n-1)}{6(n+1)^2} + \frac{n^2(n^2-1)^2}{(n^2+1)^3} \ln\left(\frac{n-1}{n+2}\right) - \frac{2n^3(n^2+2n-1)}{(n^2+1)(n^4-1)} + \frac{8n^4(n^4+1)}{(n^2+1)(n^4-1)^2} \ln(n) \quad (3)$$

where n is the ratio of refractive indices between the matrix material and the material in the pore.

Furthermore, the internal reflectivity (ρ_d) can be calculated as follows¹⁴:

$$\rho_d(n) = 1 - \frac{1 - \rho_d^{\text{ext}}}{n^2} \quad (4)$$

The refractive index of tetragonal zirconia near infrared was found to be 2.02²¹ while by definition, the refractive index of air at 1 atm is 1.0. Based on Eqs. (3) and (4), the hemispherical and internal reflectivities of zirconia coating with its pores filled by air are 38% and 85%, respectively. However, if the air inside the pore is replaced by epoxy with a refractive index of 1.66,²² the hemispherical and internal reflectivities are significantly reduced to 0.8% and 38%, respectively. This comparison suggests that reducing the refractive index mismatch will reduce the total reflection of the coating.

The above analysis agrees well with the observation on reduced reflectance of EB-PVD TBC infiltrated with epoxy (Fig. 6). During vacuum impregnation, the epoxy filled the intercolumnar gap and, hence, reduced the refractive index mismatch across the gaps. The epoxy, however, cannot infiltrate isolated pores inside the TBC columns. Thus, the reduced reflectance is only due to the reduced scattering at the TBC columns' feathery structure and intercolumnar gaps. In almost the entire wavelength range, the scattering coefficient was reduced by approximately 50% upon epoxy infiltration (Fig. 7). Similar to the case without epoxy infiltration, the scattering coefficient continued to increase as the coating thickness is reduced by polishing as a result of scattering of the isolated pores inside the columns. Thus, the contributions of the intracolumnar pores and the intercolumnar gaps to the optical scattering in an EB-PVD TBC could be distinguished.

Analogy Between Epoxy and CMAS Infiltration on TBCs

The analysis on the effect of epoxy infiltration on optical scattering is pertinent to the effect of CMAS penetration on the infrared transmission through TBCs because refractive index of the epoxy ($n = 1.66$) is almost the same as that of calcium–magnesium–alumino–silicate (CMAS, $n = 1.62$).¹¹ During service, TBC is prone to attack by CMAS due to sand ingestion into the turbine.²³ A complex thermo-mechanical–chemical interaction between CMAS and TBC leads to the failure of TBCs.^{24,25} It was also recently shown that CMAS penetration increases the infrared radiative heat transfer through the TBC so that the temperature distribution through the coating shifts to higher temperatures.¹¹ The current study suggested that the optical scattering can be reduced by replacing the air in the intercolumnar gaps with materials such as CMAS, which reduces the refractive index mismatch. Once the scattering coefficient of TBC is reduced by CMAS infiltration, the temperature inside the coatings will shift to a higher temperature due to the increase of radiative heat transfer contribution.

Evolution of Optical Scattering with Thermal Cycling

The as-received TBC coupon exhibited a low reflectance and, hence, high absorption at short wavelengths, which could be recovered upon high-

temperature exposure as short as 1 h at 1150°C in ambient atmosphere. The short wavelength absorption is attributed to the presence of a high defect concentration after coating deposition.^{26–28} It has been pointed out that delamination at the TBC/bond coat interface can also result in an increase of reflectance particularly in the mid-infrared.^{29,30} However, the contribution of local delamination to the increase of reflectance in the visible–near infrared during thermal cycle of an EB-PVD TBC at 1150°C in this work was ruled out as the reflectance is dominated by the microstructural features within the coating, as shown in Fig. 11. Essentially, the change of spectral reflectance consisted of an increase of reflectance at longer wavelength and a reflectance decrease at shorter wavelength. This was manifested by what appeared to be peak shift in the spectral reflectance, where the position of the peak shifted to a longer wavelength while the magnitude of the peak decreased with thermal cycling (Fig. 9b). As the maximum scattering occurs when the size of pores is equal to the wavelength divided by the refractive index of the material in the pores,³¹ the peak shift was attributed to the change of porosity distribution in the TBC during thermal cycling: reduction of smaller pores and increase of larger pores. This is consistent with the observation of porosity coarsening in the TBC during high-temperature aging³² and with the microstructural observation of large pores in the TBC columns after 200 1-h cycles at 1150°C (Fig. 1).

In addition to the evolution of pore size, the shape of porosity also undergoes a significant change with thermal exposure. It has been shown that the initial feathery structure of the TBC columns quickly evolves to a smoother surface.³³ Recent observation also suggested that the prolate spheroidal pores aligned to the feathery structure undergo spheroidization, leading to isolated spherical pores.³⁴ It is worth mentioning that the change of porosity distribution upon thermal cycling at 1150°C, however, is found not to change the density of the TBC.³⁵

Concluding Remarks

We have explored the effect of TBC microstructure on diffuse optical scattering in the coating and shown that the reflectance of EB-PVD TBC is primarily controlled by the refractive index mismatch between zirconia and air at the intracolumnar pores and at the

intercolumnar gaps. It was also observed that the scattering coefficient in an EB-PVD TBC is dependent on the TBC thickness with a larger scattering coefficient near the bottom of the TBC due to the smaller column size and fine scale spheroidal pores aligned to the feathery structure.

Reducing the optical mismatch at the intercolumnar gap by infiltrating the coating with an epoxy resulted in a lower scattering and, hence, a lower optical reflectance. As CMAS has a similar refractive index to that of the epoxy, it is likely that TBC attack by CMAS penetration will also reduce the optical scattering and hence detectable by diffuse optical scattering. The reduced optical scattering will also have the effect of increasing radiative heat transport through the coating leading to a higher temperature of the underlying superalloy. Thermal cycling at 1150°C was shown to alter the spectral reflectance of TBC. Optical scattering is enhanced at larger wavelength and is reduced at lower wavelength. This phenomenon was observed as a peak shift in the spectral reflectance upon thermal cycling, which was attributed to the change of porosity distribution in the TBC during thermal cycling.

As the thermal protection efficiency and the strain-tolerant capability of a TBC are typically controlled by its porosity (both intracolumnar pores and intercolumnar gaps), the sensitivity of optical reflectance to the porosity opens a new approach for the nondestructive evaluation of TBC. It also has the significant advantage of being readily applied to real components with curved surfaces.

Acknowledgment

The authors thank Dr. Ken Murphy, Howmet Research Corporation, for TBC specimens investigated in this study.

References

1. C. G. Levi, "Emerging Materials and Processes for Thermal Barrier Systems," *Curr. Opin. Solid State Mater. Sci.*, 8 77–91 (2004).
2. W. D. Kingery, "Thermal Conductivity: XII, Temperature Dependence of Conductivity for Single-Phase Ceramics," *J. Am. Ceram. Soc.*, 38 [7] 251–255 (1955).
3. R. McPherson, "A Model for the Thermal Conductivity of Plasma-Sprayed Coatings," *Thin Solid Films*, 112 89–95 (1984).
4. T. J. Lu, C. G. Levi, H. N. G. Wadley, and A. G. Evans, "Distributed Porosity as a Control Parameter for Oxide Thermal Barriers Made by Physical Vapor Deposition," *J. Am. Ceram. Soc.*, 84 [12] 2937–2946 (2001).
5. J. F. Bisson, D. Fournier, M. Poulain, O. Lavigne, and R. Mevrel, "Thermal Conductivity of Yttria–Zirconia Single Crystals, Determined with Spatially

- Resolved Infrared Thermography," *J. Am. Ceram. Soc.*, 83 [8] 1993–1998 (2000).
6. J. R. Nicholls, K. J. Lawson, A. Johnstone, and D. S. Rickerby, "Methods to Reduce the Thermal Conductivity of EB-PVD TBCs," *Surf. Coat. Technol.*, 151–152 383–391 (2002).
 7. M. R. Winter and D. R. Clarke, "Oxide Materials with Low Thermal Conductivity," *J. Am. Ceram. Soc.*, 90 [2] 533–540 (2007).
 8. D. R. Clarke, "Materials Selection Guidelines for Low Thermal Conductivity Thermal Barrier Coatings," *Surf. Coat. Technol.*, 163–164 67–74 (2003).
 9. R. C. Buchanan and S. Pope, "Optical and Electrical Properties of Yttria Stabilized Zirconia (YSZ) Crystals," *J. Electrochem. Soc.*, 130 [4] 962–966 (1983).
 10. S. Wahiduzzaman and T. Morel, "Effect of Translucence of Engineering Ceramics on Heat Transfer in Diesel Engines," Oak Ridge National Laboratory Report ORNL/Sub/88-22042/2, Oak Ridge, TN, April 1992.
 11. L. Li and D. R. Clarke, "Effect of CMAS Infiltration on Radiative Transport Through an EB-PVD Thermal Barrier Coating," *Int. J. Appl. Ceram. Technol.*, 5 [3] 278–288 (2008).
 12. L. F. Gate, "The Determination of Light Absorption in Diffusing Materials by a Photon Diffusion Model," *J. Phys. D: Appl. Phys.*, 4 1049–1056 (1971).
 13. A. M. Scallan, "An Alternative Approach to the Kubelka–Munk Theory," *J. Pulp Paper Sci.*, 11 [3] 80–84 (1985).
 14. J. I. Eldridge and C. M. Spuckler, "Determination of Scattering and Absorption Coefficients for Plasma-Sprayed Yttria-Stabilized Zirconia Thermal Barrier Coatings," *J. Am. Ceram. Soc.*, 91 [5] 1603–1611 (2008).
 15. O. Unal, T. E. Mitchell, and A. H. Heuer, "Microstructures of Y_2O_3 -Stabilized ZrO_2 Electron Beam-Physical Vapor Deposition Coatings on Ni-Based Superalloys," *J. Am. Ceram. Soc.*, 77 [4] 984–992 (1994).
 16. H.-J. Ratzler-Scheibe, U. Schulz, and T. Krell, "The Effect of Coating Thickness on the Thermal Conductivity of EB-PVD PYSZ Thermal Barrier Coatings," *Surf. Coat. Technol.*, 200 5636–5644 (2006).
 17. S. G. Terry, J. R. Litty, and C. G. Levi, "Evolution of Porosity and Texture in Thermal Barrier Coatings Grown by EB-PVD," *Elevated Temperature Coatings: Science and Technology III*, eds., J. M. Hampikian and N. B. Dahorte. The Minerals, Metals and Materials Society, Warrendale, PA, 13–26, 1999.
 18. A. A. Kulkarni, H. Herman, J. Almer, U. Lienert, D. Haeffner, J. Ilavsky, S. Fang, and P. Lawton, "Depth-Resolved Porosity Investigation of EB-PVD Thermal Barrier Coatings Using High-Energy X-Rays," *J. Am. Ceram. Soc.*, 87 [2] 268–274 (2004).
 19. R. Siegel and C. M. Spuckler, "Analysis of Thermal Radiation Effects on Temperatures in Turbine Engine Thermal Barrier Coating," *Mater. Sci. Eng. A*, 245 150–159 (1998).
 20. R. Siegel and J. R. Howell, *Thermal Radiation Heat Transfer*, 4th edition, Taylor & Francis, New York, 2002.
 21. J. A. Nychka, M. R. Winter, D. R. Clarke, T. Naganuma, and Y. Kagawa, "Temperature-Dependent Optical Reflectivity of Tetragonal-Prime Yttria-Stabilized Zirconia," *J. Am. Ceram. Soc.*, 89 [3] 908–913 (2006).
 22. T. Weber, Buehler Inc., private communication.
 23. J. L. Smialek, F. A. Archer, and R. G. Garlick, "Turbine Airfoil Degradation in the Persian-Gulf War," *J. Met.*, 46 [12] 39–41 (1994).
 24. C. Mercer, S. Faulhaber, A. G. Evans, and R. Darolia, "A Delamination Mechanism for Thermal Barrier Coatings Subject to Calcium–Magnesium–Alumino–Silicate (CMAS) Infiltration," *Acta Mater.*, 53 [4] 1029–1039 (2005).
 25. S. Kraemer, J. Yang, C. G. Levi, and C. A. Johnson, "Thermochemical Interaction of Thermal Barrier Coatings with Molten CaO – MgO – Al_2O_3 – SiO_2 (CMAS) Deposits," *J. Am. Ceram. Soc.*, 89 [10] 3167–3175 (2006).
 26. J. Shinar, D. S. Tannhauser, and B. L. Silver, "ESR Study of Color Centers in Yttria Stabilized Zirconia," *Solid State Ionics*, 18 and 19 912–915 (1986).
 27. V. R. PaiVerneker, A. N. Petelin, F. J. Crowne, and D. C. Nagle, "Color-Center-Induced Band-Gap Shift in Yttria-Stabilized Zirconia," *Phys. Rev. B*, 40 [12] 8555–8557 (1989).
 28. R. Ben-Michael, D. S. Tannhauser, and J. Genossar, "ESR Centers in Reduced Stabilized Zirconia," *Phys. Rev. B*, 43 [10] 7395–7404 (1991).
 29. J. I. Eldridge, T. J. Bencic, C. M. Spuckler, J. Singh, and D. E. Wolfe, "Delamination-Indicating Thermal Barrier Coatings Using YSZ: Eu Sublayers," *J. Am. Ceram. Soc.*, 89 [10] 3246–3251 (2006).
 30. J. I. Eldridge, C. M. Spuckler, and R. E. Martin, "Monitoring Delamination Progression in Thermal Barrier Coatings by Mid-Infrared Reflectance Imaging," *Int. J. Appl. Ceram. Technol.*, 3 [2] 94–104 (2006).
 31. W. R. Blevin and W. J. Brown, "Light Scattering Properties of Pigment Suspensions," *J. Opt. Soc. Am.*, 51 [9] 975–982 (1961).
 32. A. F. Renteria and B. Saruhan, "Effect of Ageing on Microstructure Changes in EB-PVD Manufactured Standard PYSZ Top Coat of Thermal Barrier Coatings," *J. Eur. Ceram. Soc.*, 26 2249–2255 (2006).
 33. V. Lughì, V. K. Tolpygo, and D. R. Clarke, "Microstructural Aspects of the Sintering of Thermal Barrier Coatings," *Mater. Sci. Eng. A*, 368 212–221 (2004).
 34. H.-J. Ratzler-Scheibe and U. Schulz, "The Effects of Heat Treatment and Gas Atmosphere on the Thermal Conductivity of APS and EB-PVD PYSZ Thermal Barrier Coatings," *Surf. Coat. Technol.*, 201 7880–7888 (2007).
 35. T. Kakuda, A. M. Limarga, T. D. Bennett, and D. R. Clarke, "Evolution of Thermal Properties of EB-PVD TBCs with Thermal Cycling," *Acta Mater.*, (2008), in press.